THE JOURNAL OF PHYSICAL CHEMISTRY B

Article

pubs.acs.org/JPCB

# Distribution of Protein Ramachandran Psi ($\psi$) Angle Using Non-Resonance Visible Raman Scattering Measurements

Susmita Bhattacharya,[†] Sudeshna Ghosh,[‡] Nitin Kumar Pandey,[‡] Susmitnarayan Chaudhury,[‡] Swagata Dasgupta,[‡] and Anushree Roy*[,†]

[†]Department of Physics, Indian Institute of Technology, Kharagpur 721302, India

[‡]Department of Chemistry, Indian Institute of Technology, Kharagpur 721302, India

**ABSTRACT:** Knowing the distribution of Ramachandran angles helps in understanding peptide and protein backbone conformation. Empirical relations are proposed to correlate the spectral profile of the amide $III_3$ band, obtained from ultraviolet resonance Raman measurements (UVRR), with the Ramachandran dihedral psi angle distribution in small peptide and protein molecules, in different environmental conditions (Mikhonin et al. *J. Phys. Chem. B* **2006**, *110*, 1928−1943). It has also been used for more complicated structures, like large globular proteins and protein fibrils. In our work here, we use visible Raman spectra and available empirical relations to obtain similar correlations for human serum albumin, hen egg white lysozyme, and human gamma crystallin. We also report the dihedral angle distribution in fibrils and a denatured protein in an ethanol environment using the same spectroscopic technique.

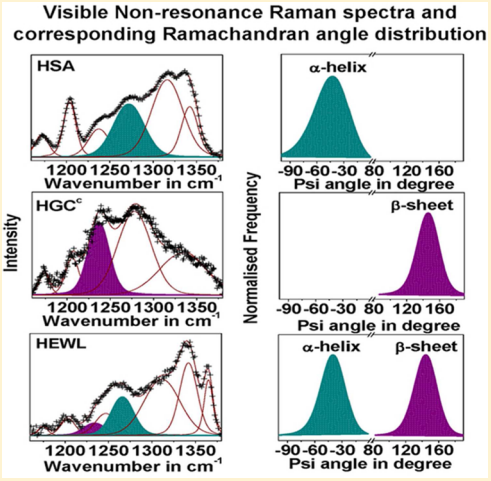


## 1. INTRODUCTION

In the last few decades, a large number of high-resolution protein structures have been determined by X-ray crystallography and included in the Protein data bank (PDB).[1] X-ray diffraction and nuclear magnetic resonance (NMR) (especially, multidimensional NMR) spectroscopy measurements are commonly used methods to determine the structures of biomolecules despite certain limitations.[2−8] Samples for which data collection is possible are required to be crystalline for X-ray diffraction and soluble for NMR. In addition, standard X-ray diffraction measurements usually obtain the information of short segments of fibrils[9−11] whereas $^{13}C$ and/or $^{15}N$ labels at specific sites are required for NMR studies.[12]

Vibrational spectroscopy provides a molecular perspective of proteins and peptides. It is especially useful to study the systems with low concentration and faster dynamics. For example, the packing defect of the compact structure of polyglutamic acid amyloid fibril has been established by vibrational circular dichroism (VCD).[13] Infrared (IR) absorption and Raman scattering measurements have been extensively used to study the structure of numerous proteins and peptides.[14−17] In 1977, R. C. Lord[18] proposed the strategic use of Raman scattering measurements to find peptide geometry. The reaction coordinate, the Ramachandran dihedral psi ($\psi$) angle of the Ramachandran plot, specifically determines the geometry of the secondary structure of proteins and peptides. Comparing the histograms of the distribution of $\psi$ angle in bovine pancreatic ribonuclease with its amide III contours in the Raman spectra, a correlation between the two was predicted.[18] A similar correlation was also suggested for lysozyme, insulin, and basic pancreatic trypsin inhibitor.[18] Polarized visible Raman spectra of the amide I band are used to determine dihedral $\phi$ and $\psi$ angles of triglycines.[19] Two parameters, one coupling the energy of the amide I band and the other determining the angle between transition dipole momenta of amide I modes, obtained from visible spectral Raman line analysis, are correlated with the Ramachandran dihedral angles of the above tripeptide.[19]

The invention of the UV laser made the possibility of such Raman studies more efficient. Under UV excitation, radiation resonance Raman scattering due to the $\pi-\pi^*$ transition[20] or preresonance enhancement due to excitonic interactions results in strong amide III bands in proteins and peptides.[20,21] A large number of reports are thus available in the literature, in which UV resonance Raman (UVRR) spectroscopy is used to study the secondary structure of the proteins.[22−28] The strong Raman spectrum of the amide III band under UV radiation opened up the possibility of linking the spectral profile with $\psi$ angle distribution quantitatively. In a study on alanine dipeptides, the dependence of the amide III band on both $\phi$ and $\psi$ angles was reported.[29] Later, it was proposed that the impact of $\phi$ angle change is relatively modest when the allowed regions of

**Received:** August 10, 2013
**Revised:** October 8, 2013
**Published:** October 17, 2013

Ramachandran angles are considered.[30] Asher et al. carried out density functional theory calculations to estimate the variation of frequency of the amide III band for different Ψ angles of isolated and hydrogen bonded alanine methyl amide (AMA).[27] Empirical relations were then proposed to correlate the Raman spectral profile of the amide $III_3$ band with Ramachandran $\psi$ angle distribution of peptides under different environmental conditions.[30] Later, these relations were also used to obtain the $\psi$ angle distribution in large peptides[25] and proteins[22,23] from the amide $III_3$ UVRR band. The conformation of the peptide backbone, using the relation between the $\psi$ angle and Raman shift of the amide $III_3$ band, was predicted for normal as well as genetically engineered amyloid fibrils.[31−33]

Following the success of UVRR spectroscopy to determine the structural conformation of proteins, a large number of reports in the literature discuss changes in photophysics and photochemistry of amino acids and proteins under UV excitation.[34,35] Thus, it is worthwhile to explore whether Raman line profiles, obtained from non-resonance visible Raman measurements, could be correlated with Ramachandran dihedral angles of proteins quantitatively. In this article, we use non-resonance Raman spectra of the amide $III_3$ band along with the relations proposed in ref 30 to correlate the spectral profile with the $\psi$ angle distribution of three proteins, $\alpha$-helix rich human serum albumin (HSA), $\beta$-sheet rich protein, cataractous human gamma crystallin ($HGC^c$), and hen-egg white lysozyme (HEWL). We propose a procedure that could be followed to analyze Raman data for such studies. In addition, we also report the distribution of the $\psi$ angle of these proteins in fibrillar and denatured states using the same spectroscopic technique.

## 2. MATERIALS AND METHODS

HSA and HEWL were purchased from Sigma Chemical Co. (St. Louis, MO). All other chemicals were obtained from SRL (India). Native proteins are dissolved in the phosphate buffer of pH 7.4. A solution of HSA in the presence of 40% ethanol (v/v) concentration was also prepared in phosphate buffer of pH 7.4. Below, we describe the methods followed for the isolation of $HGC^c$ and preparation of protein fibrils, in brief.

**$HGC^c$.** $HGC^c$ was isolated from the soluble portion of the cataractous emulsion of eye lenses. The emulsion was fractionated by size exclusion chromatography to purify the protein by removal of $\alpha$- and $\beta$-crystallins. A concentration of 30 $\mu$M of the protein in phosphate buffer of pH 7.4 has been used for the experiments reported here.

**HEWL Fibril.** The concentration of the HEWL solution in double distilled water was determined by measuring the molar extinction coefficient (37 646 $M^{-1}$ $cm^{-1}$) of the protein at 280 nm. The concentration of the solution was 150 $\mu$M. Fibrils at pH 7 were grown by heating the aqueous solution of the protein (in the presence of 80% ethanol (v/v) and 20 mM phosphate buffer of pH 7 containing 20 mM NaCl at ∼60 °C) for 6 h. Incubation of the protein results in the formation of a gel-like fraction in the solution.

**HSA Fibril.** HSA was dissolved in double distilled water, and the concentration was measured using the same procedure mentioned above. Stock solution was prepared keeping the protein concentration at 160 $\mu$M at an ethanol concentration of 60% (v/v) at pH 7.4. Fibrils were obtained by heating the stock solution at 65 °C for 6 h followed by incubation at room temperature.

The solutions were then centrifuged at 6000 rpm for 30 min to separate the fibrils. The detail protocols of preparing HSA and HEWL fibrils are available in refs 36 and 37. More details on $HGC^c$ isolation will be reported elsewhere.

**Raman Spectroscopy.** For Raman measurements, two drops of each sample were dried on a thoroughly cleaned aluminum foil at room temperature for 10 h. Raman spectra were collected with a 50× objective in backscattering geometry by using a microRaman setup equipped with an air cooled $Ar^+$ laser (model 177-G1205, Spectra Physics, USA) as the excitation light source, a single monochromator (TRIAX 550, JY, France), and a CCD detector. A low incoming laser power of 4 mW was chosen to avoid the heating effect. All reported spectra are the average of five spectra, each recorded with a 300 s integration time.

**Protein Structure Analysis.** The distributions of Ramachandran $\psi$ angle of HSA, $HGC^c$, and HEWL proteins were generated using an online web compiler, "Volume, Area, Dihedral Angle Reporter" (VADAR) (version 1.8).[38] VADAR is a program for analyzing and quantitatively estimating a large number of structural parameters of peptides and proteins from their coordinates available in their PDB file. We have used the PDB File nos. 1AO6, 1HK0, and 6LYZ for HSA, $HGC^c$, and HEWL, respectively,[39−41] of the RCSB databank.[1] PyMol[42] was used to visualize the conformations of the protein structure presented in Figure 1.

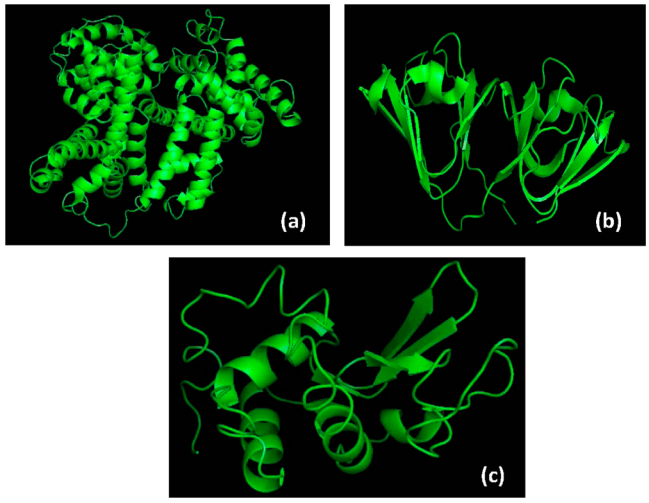


**Figure 1.** Cartoons of (a) HSA, (b) $HGC^c$, and (c) HEWL in their native structure. Figures are generated using the PyMol program and inputs from PDB files (see text).

## 3. EMPIRICAL RELATIONS TO CORRELATE AMIDE III RAMAN LINE PROFILE AND RAMACHANDRAN $\psi$ ANGLE DISTRIBUTION

Amide III vibrations of proteins mostly involve C−N stretching, N−H bending, and C−C stretching vibrations.[43,44] The complexity of the band increases due to mixing of the above normal mode vibrations with $C_{\alpha 1}H$ bending vibrations. The out of phase mixing with $C_{\alpha 1}H_{ib}$ and $C_{\alpha 1}H_{ob}$ is referred to as the amide $III_1$ band. An in-phase mixing of $C_{\alpha 2}H$ also contributes to this band. The amide $III_2$ band involves in-phase mixing of $NH_{1b}$ and $C_{\alpha 1}H_{ib}$. All four $C_\alpha H$ bending modes contribute to the amide $III_3$ band.[44] In a Raman spectrum, these three amide III sub-bands are centered at 1337, 1303, and 1261 $cm^{-1}$. Here we have followed the notation in refs 24 and 28.

The Ramachandran $\psi$ angle describes the rotation of polypeptide backbone around the bonds between $C_\alpha$−H and C. The van der Waals interaction of hydrogen atoms of $C_\alpha$−H and N−H bonds affects the positive $\psi$ angle. As all four types of $C_\alpha H$ bending modes are involved in the amide $III_3$ band, the coupling of these two vibrational modes ($C_\alpha$−H and N−H) results in dihedral angle dependence of the vibrational frequency of the amide $III_3$ band in proteins and peptides. The frequency of the amide $III_3$ band also depends on the presence of peptide−peptide hydrogen bonds ($HB_{p-p}$), peptide−water hydrogen bonds ($HB_{p-w}$), and temperature ($T$), $\nu_{III} = \nu_{III}(\phi, \psi, HB_{p-p}, HB_{p-w}, T)$. It is shown that the dependence of $\nu_{III}$ is much less for the phi ($\phi$) angle in comparison to the $\psi$ angle.[27,45] Mikhonin et al.[30] established sinusoidal correlations between $\nu_{III}$ and $\psi$ in the form of $\nu_{III}(\psi) \cong \nu_o + \sin(\psi - \alpha_0)$ by calculating the former for different conformations of varying $\psi$ angle of different peptides in a vacuum. Further, it is assumed that the dependence of the amide $III_3$ frequency to hydrogen bonding and temperature is added linearly in the above equation as[30]

$$\upsilon_{III}(\psi, HB_{p-p}, HB_{p-w}, T) = \{\upsilon_0 - A \sin(\psi - \alpha_0)\} + \Delta\upsilon_{III}(HB_{p-p}, HB_{p-w}, T) \quad (1)$$

The amide $III_3$ frequencies in the UVRR spectra of polypeptides with $\alpha$-helix, $2.5_1$-helix, and $\beta$-sheet structures in different environmental conditions were measured. Empirical relations correlating the frequency of the amide III band and the $\psi$ angle in different conformations of small peptides under different environmental conditions were then proposed. For a $\beta$-sheet in water with PB−PB hydrogen bonding, eq 1 modifies as[30,31]

$$\upsilon_{III}(\psi, HB) = \{1244\ cm^{-1} - 54\ cm^{-1} \sin(\psi + 26)\} \quad (2a)$$

For PPII-like and $2.5_1$-helix-like conformations of peptides exposed in a water environment, eq 1 is modified as[30,33]

$$\upsilon_{III}(\psi, HB) = \{1256\ cm^{-1} - 54\ cm^{-1} \sin(\psi + 26)\} \quad (2b)$$

In eq 2, the effect of temperature is neglected, as its contribution is negligible for room temperature. The maximum error in estimating the value of the $\psi$ angle using these empirical relations is claimed to be not more than ±14°.[30]

## 4. RESULTS AND DISCUSSION

Figure 2 shows the non-resonance Raman spectra of six different samples—HGC[c], HSA, HEWL, HSA and HEWL fibrils, and denatured HSA in 40% ethanol solution—over the spectral window from 400 to 1400 $cm^{-1}$.

The secondary structure of HGC[c] is dominated by a $\beta$-sheet component (Figure 1a),[46] while HSA consists of 69% $\alpha$-helix, with the remaining structures being either turns or disordered structures (Figure 1b).[41] Like HSA, HEWL is also a globular protein. It comprises 42% $\alpha$-helix, 7% $\beta$-sheet, and 22% disordered structure (Figure 1c).[47] To investigate the amide III band, we have analyzed the broad spectral window over the range between 1160 and 1380 $cm^{-1}$. For uniformity, a linear background has been subtracted from all spectra in this range. Figure 3 shows the background subtracted spectra of the amide III region for all samples under study. Other than the contribution of the secondary structural components, the

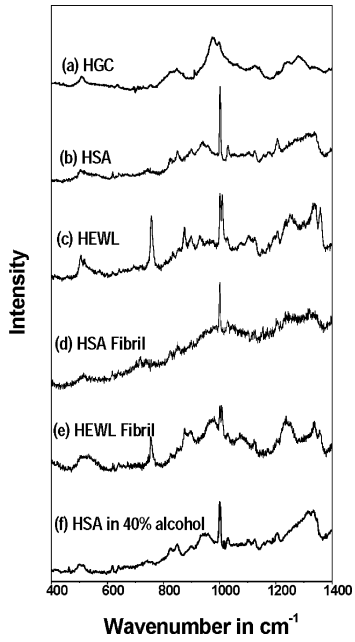


**Figure 2.** Raman spectra of (a) HGC[c], (b) HSA, (c) HEWL, (d) HSA fibril, (e) HEWL fibril, and (f) HSA in 40% (v/v) ethanol solution over the spectral range 400−1400 $cm^{-1}$.

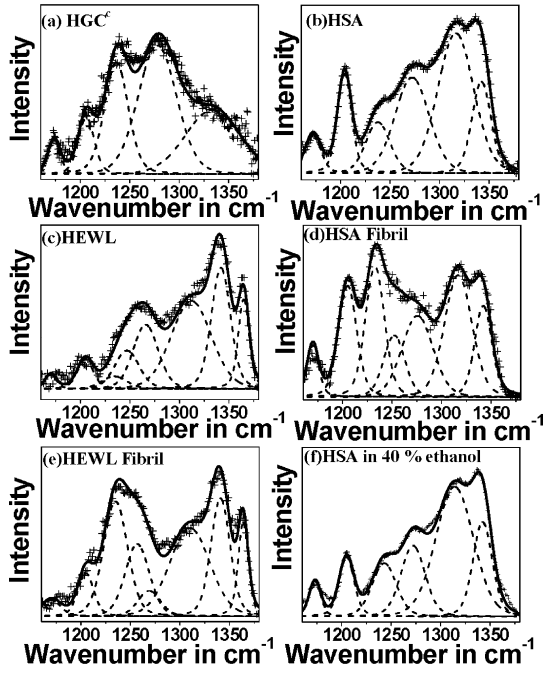


**Figure 3.** Raman spectra between 1160 and 1380 $cm^{-1}$ for (a) HGC[c], (b) HSA, (c) HEWL, (d) HSA fibril, (e) HEWL fibril, and (f) HSA in 40% (v/v) ethanol solution. Deconvoluted components are shown by dashed lines and net fitted spectra by solid lines. The experimental data points are shown by + symbols.

analyzed spectral range carries the signature of various other vibrational modes of the specific molecule. Thus, the deconvolution of each spectral profile has been carried out with extra precaution. The presence of different types of a particular secondary structure (e.g., parallel and antiparallel $\beta$-sheets, short helixes in globular proteins) results in an anisotropic Raman line profile.[15] However, the spectral profile of a protein can be analyzed with reasonable precision using


dx.doi.org/10.1021/jp408009y | J. Phys. Chem. B 2013, 117, 13993−14000

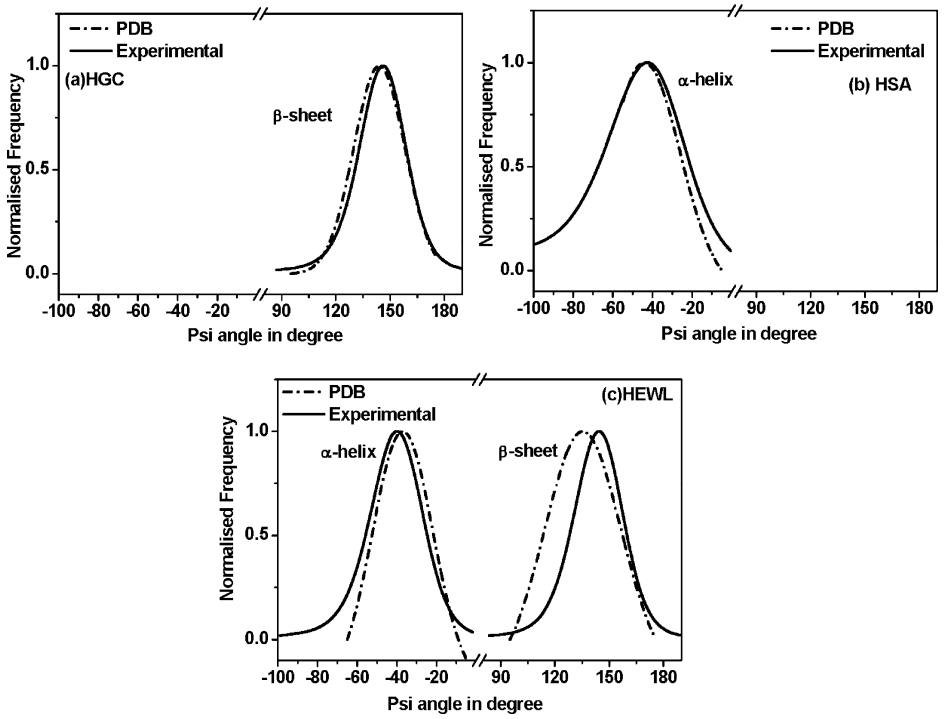


**Figure 4.** Distribution of protein Ramachandran $\psi$ angle, (a) HGC$^c$, (b) HSA, and (c) HEWL, as obtained from deconvolution of the amide III band. Experimentally obtained distributions are shown by the solid lines. Distributions generated from the PDB file of the corresponding structure are shown by the dotted lines.

Voigt functions.[16,48] Moreover, as we are analyzing broad overlapping bands and the asymmetry of each component is unknown, we refrain from using the asymmetric function to avoid additional error. The intensity of each spectrum with $n$ number of components in Figure 3 is fitted with[49]

$$I = \sum_n A_n \frac{2\ln 2}{\pi^{3/2}} \frac{\Gamma_{Ln}}{\Gamma_{Gn}} \int_{-\infty}^{\infty} \frac{e^{-t^2}}{\left(\sqrt{2\ln 2}\frac{\Gamma_{Ln}}{\Gamma_{Gn}}\right)^2 + \left(\sqrt{4\ln 2}\frac{\omega-\omega_{0n}}{\Gamma_{Gn}} - t\right)^2} dt \quad (3)$$

where $\Gamma_{Ln}$ and $\Gamma_{Gn}$ are parameters in the full Voigt profile. These two parameters correspond to the full width at half-maximum of the Lorentzian and Gaussian components, used while defining any general Voigt function. $\omega_{0n}$ is the central frequency of the Voigtian profile. $A_n$ is a constant.

In the above fitting procedure, we have imposed the following constraints: (i) The integral intensity ratios of secondary structural components are kept close to their expected relative fractions in the proteins (for HSA disordered structure: $\alpha$-helix = 1:2.2 (from X-ray diffraction measurements); 1:2.6 from CD measurements;[50] and for HEWL $\beta$-sheet:disordered structure:$\alpha$-helix = 1:3:6[47]). (ii) Three main secondary structures—$\beta$-sheet, disordered structure, and $\alpha$-helix—of a protein in the amide III$_3$ band contribute in the range 1235−1242, 1242−1250, and 1260−1310 cm$^{-1}$, respectively.[51] The peak positions due to these secondary structures were allowed to vary only in the allowed range of the wavenumber mentioned above. (iii) Other than expected Raman bands due to the secondary structural component of the protein, we added the minimum number of spectral components for the deconvolution to obtain the best fit curve. These constraints are strictly followed in the deconvolution procedure. In the case of HGC$^c$, the spectral range between 1160 and 1380 cm$^{-1}$ is deconvoluted with five Voigt functions with peak wavenumbers at 1168, 1205, 1236, 1278, and 1333 cm$^{-1}$. In addition to the Raman band due to $\beta$-sheet at 1236 cm$^{-1}$, two broad bands at ∼1278 and ∼1333 cm$^{-1}$ appear in the spectra. These two peaks may be due to $CH_2$ and $CH_\alpha$ in-plane bending vibrations in the molecule.[52] The Raman lines at 1168 and 1205 cm$^{-1}$ are assigned to vibrational modes of Tyr, Phe/Tyr residues.[53] The Raman spectrum of HSA in the above range is deconvoluted with six Voigt functions with mean peak wavenumbers at 1168, 1204, 1244, 1271, 1320, and 1345 cm$^{-1}$. Other than Raman bands of residues and C−H, as observed for HGC$^c$, the new modes at 1244 and 1271 cm$^{-1}$ are due to disordered structures and $\alpha$-helical secondary structures of the protein. The ratio of the integral intensities of these two peaks is 1:2.7. The relatively sharp Raman band at 1345 cm$^{-1}$ originates from the Trp residue of the molecule.[54] A similar deconvolution procedure is followed for the Raman spectrum of the HEWL molecule (Figure 3c). In this case, the integral intensity ratio of $\beta$-sheet:disordered structure:$\alpha$-helix is 1:3:5. All types of structural features—$\alpha$-helix, $\beta$-sheet, and disordered structure—contribute to the spectrum of the protein.

Here we would like to mention that, for a large protein molecule (like HSA and HEWL), overlap of different Raman bands is unavoidable either in non-resonance or resonance spectra.[31,33] Moreover, in the above analysis, we did not include the contribution of amide III$_1$ and amide III$_2$ bands in the spectra. The amide III$_3$ band, termed as the "classical amide III band", is usually the most intense.[24] Nonetheless, the possibility of overlap between them in the case of visible Raman measurements of large protein molecules turns the analysis of

the amide III spectra nontrivial. Thus, the deconvolution procedure, mentioned above, is to be strictly followed to avoid the effect of the overlapping bands.

The distribution of the $\psi$ angle in HGC[c], HSA, and HEWL native proteins using the spectral profile of $\alpha$-helix and/or $\beta$-sheet components as obtained from the above deconvolution procedure and the relations in eq 2 are shown in Figure 4 by solid lines. The same distributions obtained from the PDB file of the native proteins are shown by the dotted lines in the respective figures. A comparison between the estimated mean value and uncertainty (width of the Voigt profile) of the $\psi$ angle with the same obtained from PDB file is available in Table 1.

**Table 1. Distribution of Protein Ramachandran $\psi$ angle as Obtained from PDB File and Visible Raman Spectroscopic Technique[a]**

| | Ramachandran angle for helix content | | | | Ramachandran angle for sheet content | | | |
|---|---|---|---|---|---|---|---|---|
| | from PDB files | | from Raman measurements | | from PDB files | | from Raman measurements | |
| proteins under study | mean | $2\sigma$ | mean | $2\sigma$ | mean | $2\sigma$ | mean | $2\sigma$ |
| HGC[c] | | | | | 144 | 28 | 146 | 26 |
| HSA | −44 | 36 | −44 | 39 | | | | |
| HEWL | −37 | 30 | −40 | 26 | 135 | 42 | 144 | 27 |
| HSA fibril | | | −48 | 36 | | | 141 | 21 |
| HEWL fibril | | | −37 | 27 | | | 143 | 27 |
| HSA in 40% ethanol | | | −44 | 27 | | | | |

[a] $\sigma$ is the standard deviation obtained assuming the distribution to be Gaussian.

For HGC[c], the experimentally obtained mean value of $\psi$ for $\beta$-sheet was found to be 146° (Figure 4a), which is very close to the value 144° reported for $\beta$-sheet in the PDB file.[40] For HSA, the mean value of $\psi$ for the $\alpha$-helical component is reported to be −44° in the PDB file;[39] the experimentally generated value is the same. For HEWL, experimentally observed mean values of $\psi$ angles for the $\alpha$-helix and $\beta$-sheet (−40 and 144°) also match quite well with those available in the PDB file (−37 and 135°),[41] as shown in Figure 4c. In all cases, the difference in mean values between the estimated and those obtained from the PDB file is within the expected experimental error (±14°). For most of the globular proteins, the difference in average torsion $\psi$ angle of parallel and antiparallel $\beta$-sheet is ∼8° with a standard deviation of 15° for each component.[55] Individually, they must contribute to different dihedral angle distributions. We believe that, though non-resonance Raman spectra of the amide $III_3$ band can be used to estimate average $\psi$ angle distributions, the technique is not sensitive to study such finer differences in peptide/protein conformation, which could be investigated by UVRR measurements.[43] In the above, we find that it is possible to measure the absolute value of mean $\psi$ angle using non-resonance Raman measurements. The notable error bar (±14°) is inherent in the technique of estimating $\psi$ angle distribution using the empirical relations and the spectral profile.[30] Within these experimental limitations, we use the above technique for estimation of the distribution of dihedral angle in HSA and HEWL fibrils. The effect of denaturation of the HSA in 40% ethanol environment also has been investigated. Though the distribution of dihedral angles in short peptide segments of amyloid fibrils is available in the literature,[11,56] the quantitative estimation of the same for the whole molecule is nontrivial by X-ray diffraction measurement.

**HSA and HEWL Fibrils.** Fibril formation is related to prominent secondary structural changes in the protein molecule. Transitions from $\alpha$-helix to $\beta$-sheet and aggregation of protein molecules lead to fibril formation.[57] Raman spectra of HSA and HEWL fibrils over the range between 1160 and 1380 $cm^{-1}$ are analyzed (Figure 3d and f). Here, the important point to note is that the background subtraction, deconvolution of Raman spectra of structurally modified protein, is carried out following the same procedure and using the same constraints, mentioned earlier for the corresponding native protein. The ratio of the integral intensity of $\beta$-sheet:disordered structure:$\alpha$-helical components is kept at 2:1:2 for HSA and 5:3:1 HEWL fibrils. The ratios of $\beta$-sheet:$\alpha$-helical components are very close to the values for these fibrils reported from CD measurements.[36,37] Hence, the distributions of $\psi$ angles related to $\alpha$-helix and $\beta$-sheet are obtained. In Figure 5, the solid line describes the distribution of $\psi$ angle in HSA and HEWL native proteins (as obtained earlier), while the dotted line describes the same for their fibrillar state. The mean $\psi$ angles for the $\alpha$-helix and $\beta$-sheet are at −48 and 141° in HSA fibrils (Figure 5a), while the distributions are centered at −37 and 143° for HEWL fibrils (Figure 5b). We find that the distributions of $\psi$ angle related to $\alpha$-helix and $\beta$-sheet in HEWL fibrils are very similar to those of native proteins. For HSA fibril, the above spectroscopic analysis reveals the $\psi$ angle distribution related to $\beta$-sheet content. To the best of our knowledge, this structural information on HSA fibrils was unknown until now.

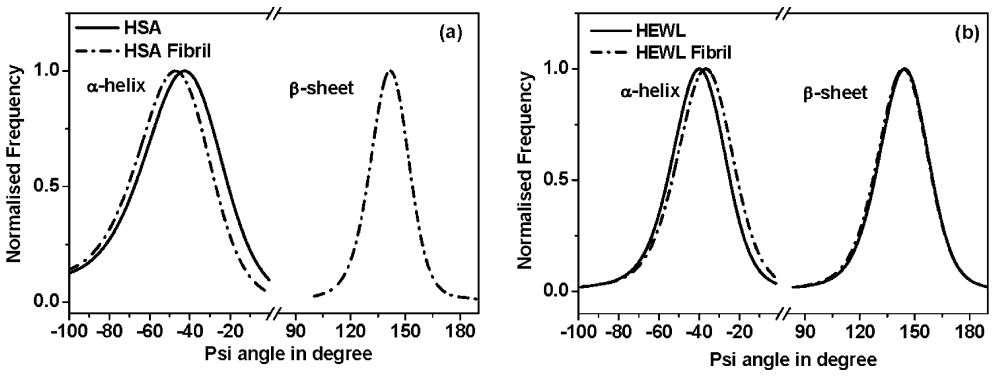


**Figure 5.** Distribution of Ramachandran $\psi$ angle for protein (solid lines) and its fibrils (dotted lines): (a) HSA; (b) HEWL.


dx.doi.org/10.1021/jp408009y | J. Phys. Chem. B 2013, 117, 13993−14000

**Denatured Proteins.** Proteins in alcohol mimic the environment of biomembrane.[58] Low polarity of the alcohol molecules modifies the pathway of protein folding.[59−64] Alcohol increases the hydrophobicity at the peptide−solvent interface by displacing water in the peptide hydration shell.[65] However, it increases the interaction strength of hydrogen bonds, which results in stabilization of secondary structure, especially $\alpha$-helix. The solvation process is favored only if the overall Gibbs free energy of the solution is decreased. The native structure of a protein is related to one of the minimum energy states of the protein. In the presence of excess alcohol, proteins are found to acquire a non-native state which is energetically favored with a change in distribution in $\psi$ angle.[25,66] It is to be noted that the protein conformation strongly depends on alcohol concentration.[67] We have plotted the variation of $\psi$ angle for HSA in the presence of 40% of ethanol (v/v) concentration (dotted line), as obtained from similar Raman spectral analysis (Figure 3f), with that of the native protein (solid line in Figure 6). The ratio of the integral

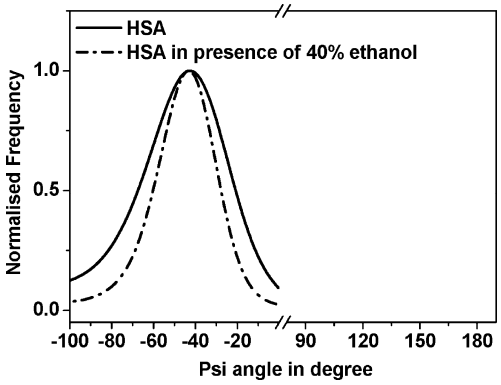


**Figure 6.** Change in distribution of $\psi$ angle in the presence of alcohol as a measure of protein denaturation HSA. The solid line shows the distribution for 0% ethanol, while the dotted line shows the same for 40% (HSA) ethanol.

intensity of disordered structure:$\alpha$-helix is 1:1 for HSA in 40% ethanol[57] environment. We find that, though the mean $\psi$-value for the $\alpha$-helix remains the same, the width of the distribution clearly decreases in an ethanol environment. Circular dichroism (CD) and UV−vis spectroscopic measurements reveal that, at ethanol concentrations between 30 and 50%, the $\alpha$-helical component of HSA molecules transformed into mixed $\beta$ structure and disordered conformation.[67] Thermodynamically, it has been shown that such conformational changes result in modified specific volume and compressibility of the HSA molecule.[67] From our analysis, the ratio of $\alpha$-helix in native and denatured HSA in 40% ethanol environment is nearly 2:1. Thus, indeed, one expects the decrease in the distribution of the $\psi$ angle in the latter case. A narrower distribution of $\psi$ angle in thermally denatured protein is reported from UVRR measurements[66] and has been related to the decrease in the helical component in this system.

## 5. SUMMARY

Non-resonance visible Raman spectroscopy is known to be a powerful nondestructive tool to get quantitative information regarding the backbone conformation of large proteins and their fibrils. In this article, we have shown that this spectroscopic technique can be used to obtain the distribution of dihedral $\psi$ angle in proteins. We propose a method for analyzing the Raman band of amide $III_3$ using the known ratio of different secondary structural components, to obtain the distribution of dihedral angle in large protein molecules. The experimental results for HSA, HEWL, and $HGC^c$ molecules match quite well with the crystallographically obtained data from the PDB files. We also report the $\psi$ angle distribution of the proteins in fibrillar or denatured states. We believe that this method of analysis is a direct spectroscopic approach for predicting the backbone conformation of large protein molecules and its fibrils and may be considered as a biocompatible alternative of UVRR measurements in structural biology.

## AUTHOR INFORMATION

### Corresponding Author

*E-mail: anushree@phy.iitkgp.ernet.in. Phone: +91-3222-283856. Fax: +91-3222-255303.

### Notes

The authors declare no competing financial interest.

## REFERENCES

(1) Berman, M.; Westbrook, J.; Feng, Z.; Gilliland, G.; Bhat, T. N.; Weissig, H.; Shindyalov, I. N.; Bourne, P. E. The Protein Data Bank. *Nucleic Acids Res.* **2000**, *28*, 235−242.

(2) Fujii, K.; Young, M. T.; Harris, K. D.M. Exploiting Powder X-ray Diffraction for Direct Structure Determination in Structural Biology: The P2 × 4 Receptor Trafficking Motif YEQGL. *J. Struct. Biol.* **2011**, *174*, 461−467.

(3) Hunter, M. S.; DePonte, D. P.; Shapiro, D. A.; Kirian, R. A.; Wang, X.; Starodub, D.; Marchesini, S.; Weierstall, U.; Doak, R. B.; Spence, J. C. H.; Fromme, P. X-ray Diffraction from Membrane Protein Nanocrystals. *Biophys. J.* **2011**, *100*, 198−206.

(4) Abskharon, R. N. N.; Soror, S. H.; Pardon, E.; Hassan, H. E.; Legname, G.; Steyaerta, J.; Wohlkoniga, A. Crystallization and Preliminary X-Ray Diffraction Analysis of a Specific VHH Domain against Mouse Prion Protein. *Acta Crysttalogr., Sect. F* **2010**, *66*, 1644−1646.

(5) Clore, G. M.; Gronenborn, A. M. New Methods of Structure Refinement for Macromolecular Structure Determination by NMR. *Proc. Natl. Acad. Sci. U.S.A.* **1998**, *95*, 5891−5898.

(6) Wider, G.; Wuthrich, K. NMR Spectroscopy of Large Molecules and Multimolecular Assemblies in Solution. *Curr. Opin. Struct. Biol.* **1999**, *9*, 594−601.

(7) Tugarinov, V.; Hwang, P. M.; Kay, L. E. Nuclear Magnetic Resonance Spectroscopy of High Molecular Weight Proteins. *Annu. Rev. Biochem.* **2004**, *73*, 107−146.

(8) Dyson, H. J.; Wright, P. E. Unfolded Proteins and Protein Folding Studied by NMR. *Chem. Rev.* **2004**, *104*, 3607−3622.

(9) Inouye, H.; Sharma, D.; Goux, W. J.; Kirschner, D. A. Structure of Core Domain of Fibril-Forming PHF/Tau Fragments. *Biophys. J.* **2006**, *90*, 1774−1789.

(10) Nelson, R.; et al. Structure of the Cross-$\beta$ Spine of Amyloid-Like Fibrils. *Nature* **2005**, *435*, 773−778.

(11) Sawaya, M. R.; et al. Atomic Structures of Amyloid Cross-$\beta$ Spines Reveal Varied Steric Zippers. *Nature* **2007**, *447*, 453−457.

(12) Tycko, R. Molecular Structure of Amyloid Fibrils: Insights from Solid-state NMR. *Q. Rev. Biophys.* **2006**, *39*, 1−55.

(13) Fulara, A.; Lakhani, A.; Wójcik, S.; Nieznańska, H.; Keiderling, T. A.; Dzwolak, W. Spiral Superstructures of Amyloid-Like Fibrils of Polyglutamic Acid: An Infrared Absorption and Vibrational Circular Dichroism Study. *J. Phys. Chem. B* **2011**, *115*, 11010−11016.

(14) Ren, H.; Jiang, J.; Mukamel, S. Deep UV Resonance Raman Spectroscopy of $\beta$-Sheet Amyloid Fibrils: A QM/MM Simulation. *J. Phys. Chem. B* **2011**, *115*, 13955−13962.

(15) Schweitzer-Stenner, R. Secondary Structure Analysis of Polypeptides Based on an Excitonic Coupling Model to Describe the Band Profile of Amide Í of IR, Raman, and Vibrational Circular Dichroism Spectra. *J. Phys. Chem. B* **2004**, *108*, 16965−16975.
(16) Schweitzer-Stenner, R. Simulated IR, Isotropic and Anisotropic Raman, and Vibrational Circular Dichroism Amide I Band Profiles of Stacked β-Sheets. *J. Phys. Chem. B* **2012**, *116*, 4141−4153.
(17) Zou, Y.; Li, Y.; Hao, W.; Hu, X.; Ma, G. Parallel β-Sheet Fibril and Antiparallel β-Sheet Oligomer: New Insights into Amyloid Formation of Hen Egg White Lysozyme under Heat and Acidic Condition from FTIR Spectroscopy. *J. Phys. Chem. B* **2013**, *117*, 4003−4013.
(18) Lord, R. C. Strategy and Tactics in the Raman Spectroscopy of Biomolecules. *Appl. Spectrosc.* **1977**, *31*, 187−194.
(19) Schweitzer-Stenner, R.; Eker, F.; Huang, Q.; Griebenow, K. Dihedral Angles of Trialanine in $D_2O$ Determined by Combining FTIR and Polarized Visible Raman Spectroscopy. *J. Am. Chem. Soc.* **2001**, *123*, 9628−9633.
(20) Dudik, J. M.; Johnson, C. R.; Asher, S. A. UV Resonance Raman Studies of Acetone, Acetamide, and N-Methylacetamlde: Models for the Peptide Bond. *J. Phys. Chem.* **1985**, *89*, 3805−3814.
(21) Pajcini, V.; Asher, S. A. Preresonance Raman Single-Crystal Measurements of Electronic Transition Moment Orientations in *N*-Acetylglycinamide. *J. Am. Chem. Soc.* **1999**, *121*, 10942−10954.
(22) Chi, Z.; Chen, X. G.; Holtz, J. S. W.; Asher, S. A. UV Resonance Raman-Selective Amide Vibrational Enhancement: Quantitative Methodology for Determining Protein Secondary Structure. *Biochemistry* **1998**, *37*, 2854−2864.
(23) Copeland, R. A.; Spiro, T. G. Secondary Structure Determination in Proteins from Deep (192−223-nm) Ultraviolet Raman Spectroscopy. *Biochemistry* **1987**, *26*, 2134−2139.
(24) Mikhonin, A. V.; Ahmed, Z.; Ianoul, A.; Asher, S. A. Assignments and Conformational Dependencies of the Amide III Peptide Backbone UV Resonance Raman Bands. *J. Phys. Chem. B* **2004**, *108*, 19020−19028.
(25) Asher, S. A.; Mikhonin, A. V.; Bykov, S. UV Raman Demonstrates that α-Helical Polyalanine Peptides Melt to Polyproline II Conformations. *J. Am. Chem. Soc.* **2004**, *126*, 8433−8440.
(26) Cai, S.; Singh, B. R. A Distinct Utility of the Amide III Infrared Band for Secondary Structure Estimation of Aqueous Protein Solutions Using Partial Least Squares Methods. *Biochemistry* **2004**, *43*, 2541−2549.
(27) Asher, S. A.; Ianoul, A.; Mix, G.; Boyden, M. N.; Karnoup, A.; Diem, M.; Schweitzer-Stenner, R. Dihedral Ψ Angle Dependence of the Amide III Vibration: A Uniquely Sensitive UV Resonance Raman Secondary Structural Probe. *J. Am. Chem. Soc.* **2001**, *123*, 11775−11781.
(28) Mikhonin, A. V.; Asher, S. A. Uncoupled Peptide Bond Vibrations in α-Helical and Polyproline II Conformations of Polyalanine Peptides. *J. Phys. Chem. B* **2005**, *109*, 3047−3052.
(29) Mirkin, N. G.; Krimm, S. Amide III Mode φ, ψ Dependence in Peptides: A Vibrational Frequency Map. *J. Phys. Chem. A* **2002**, *106*, 3391−3394.
(30) Mikhonin, A. V.; Bykov, S. V.; Myshakina, N. S.; Asher, S. A. Peptide Secondary Structure Folding Reaction Coordinate: Correlation between UV Raman Amide III Frequency, Ψ Ramachandran Angle, and Hydrogen Bonding. *J. Phys. Chem. B* **2006**, *110*, 1928−1943.
(31) Xu, M.; Shashilov, V.; Lednev, I. K. Genetic Engineering Combined with Deep UV Resonance Raman Spectroscopy for Structural Characterization of Amyloid-like Fibrils. *J. Am. Chem. Soc.* **2007**, *129*, 11002−11003.
(32) Sikirzhytski, V.; Topilina, N. I.; Higashiya, S.; Welch, J. T.; Lednev, I. K. Genetic Engineering Combined with Deep UV Resonance Raman Spectroscopy for Structural Characterization of Amyloid-like Fibrils. *J. Am. Chem. Soc.* **2008**, *130*, 5852−5853.
(33) Xiong, K.; Punihaole, D.; Asher, S. A. UV Resonance Raman Spectroscopy Monitors Polyglutamine Backbone and Side Chain Hydrogen Bonding and Fibrillization. *Biochemistry* **2012**, *51*, 5822−5830.
(34) Neves-Petersen, M. T.; Gajula, G. P.; Petersen, S. B. UV light effects on proteins: from photochemistry to nanomedicine. In *Molecular Photochemistry—Various Aspects*; Saha, S., Ed.; InTech: Rijeka, Croatia, **2012**. DOI: 10.5772/2058.
(35) Sweeney, J. A.; Asher, S. A. Tryptophan UV-resonance Raman Excitation Profile. *J. Phys. Chem.* **1990**, *94*, 4784−4791.
(36) Pandey, N. K.; Ghosh, S.; Dasgupta, S. Fibrillation in Human Serum Albumin is Enhanced in the Presence of Copper(II). *J. Phys. Chem. B* **2010**, *114*, 10228−10233.
(37) Ghosh, S.; Pandey, N. K.; Bhattacharya, S.; Roy, A.; Dasgupta, S. Fibrillation of Hen Egg White Lysozyme Triggers Reduction of Copper(II). *Int. J. Biol. Macromol.* **2012**, *51*, 1−6.
(38) http://vadar.wishartlab.com/.
(39) Sugio, S.; Kashima, A.; Mochizuki, S.; Noda, M.; Kobayashi, K. Crystal Structure of Human Serum Albumin at 2.5Å Resolution. *Protein Eng.* **1999**, *12*, 439−446.
(40) Basak, A. K.; Bateman, O.; Slingsby, C.; Pande, A.; Asherie, N.; Ogun, O.; Benedek, G.; Pande, J. High-resolution X-ray Crystal Structures of Human γDCrystallin (1.25 Á) and the R58H Mutant (1.15 Á) Associated with Aculeiform Cataract. *J. Mol. Biol.* **2003**, *328*, 1137−1147.
(41) Diamond, R. Real-space Refinement of the Structure of Hen Egg-white Lysozyme. *J. Mol. Biol.* **1974**, *82*, 371−391.
(42) Delano, W. L. *The PyMOL molecular graphics system*; DeLano Scientific: San Carlos, CA, 2004.
(43) Popova, L. A.; Kodali, R.; Wetzel, R.; Lednev, I. K. Structural Variations in the Cross-β Core of Amyloid β Fibrils Revealed by Deep UV Resonance Raman Spectroscopy. *J. Am. Chem. Soc.* **2010**, *132*, 6324−6328.
(44) Schweitzer-Stenner, R.; Eker, F.; Huang, Q.; Griebenow, K.; Mroz, P. A.; Kozlowski, P. M. Structure Analysis of Dipeptides in Water by Exploring and Utilizing the Structural Sensitivity of Amide III by Polarized Visible Raman, FTIR-Spectroscopy and DFT Based Normal Coordinate Analysis. *J. Phys. Chem. B* **2002**, *106*, 4294−4304.
(45) Ianoul, A.; Boyden, M. N.; Asher, S. A. Dependence of the Peptide Amide III Vibration on the Φ Dihedral Angle. *J. Am. Chem. Soc.* **2001**, *123*, 7433−7434.
(46) Nai-Teng, Yu; East, E. J. Laser Raman Spectroscopic Studies of Ocular Lens and its Isolated Protein Fractions. *J. Biol. Chem.* **1975**, *250*, 2196−2202.
(47) Greenfield, N. J. Using Circular Dichroism Spectra to Estimate Protein Secondary Structure. *Nat. Protoc.* **2006**, *1*, 2876−2890.
(48) Eker, F.; Cao, X.; Nafie, L.; Schweitzer-Stenner, R. Tripeptides Adopt Stable Structures in Water. A Combined Polarized Visible Raman, FTIR, and VCD Spectroscopy Study. *J. Am. Chem. Soc.* **2002**, *124*, 14330−14341.
(49) He, J.; Zhang, Q. An exact calculation of the Voigt spectral line profile in spectroscopy. *J. Opt. A: Pure Appl. Opt.* **2007**, *9*, 565−568.
(50) Juárez, J.; Goy López, S.; Cambón, A.; Taboada, P.; Mosquera, V. Influence of Electrostatic Interactions on the Fibrillation Process of Human Serum Albumin. *J. Phys. Chem. B* **2009**, *113*, 10521−10529.
(51) Ishizaki, H.; Balaram, P.; Nagaraj, R.; Venkatachalapathi, Y. V.; Tu, A. T. Determination of β-Turn Conformation by Laser Raman Spectroscopy. *Biophys. J.* **1981**, *36*, 509−517.
(52) Ed. Rehman, I. U.; Movasaghi, Z.; Rehman. S. *Vibrational Spectroscopy for Tissue Analysis*; CRC Press: Orlando, FL, USA, 2013.
(53) Chen, M. C.; Lord, R. C.; Mendelsohn, R. J. Laser-Excited Raman Spectroscopy of Biomolecules.V. Conformational Changes Associated with the Chemical Denaturation of Lysozyme. *J. Am. Chem. Soc.* **1974**, *96*, 3038−3042.
(54) Tuma, R. Raman Spectroscopy of Proteins: from Peptides to Large Assemblies. *J. Raman Spectrosc.* **2005**, *36*, 307−319.
(55) Hovmöller, S.; Zhou, T.; Ohlson, T. Conformations of Amino Acids in Proteins. *Acta Crystallogr., Sect. D* **2002**, *58*, 768−776.
(56) Jaroniec, C. P.; MacPhee, C. E.; Astrof, N. S.; Dobson, C. M.; Griffin, R. G. Molecular Conformation of a Peptide Fragment of

Transthyretin in an Amyloid Fibril. *Proc. Natl. Acad. Sci. U.S.A.* **2002**, *99*, 16748−16753.
(57) Juárez, J.; Alatorre-Meda, M.; Cambón, A.; Topete, A.; Barbosa, S.; Taboada, P.; Mosquera, V. Hydration Effects on the Fibrillation Process of a Globular Protein: The Case of Human Serum Albumin. *Soft Matter* **2012**, *8*, 3608−3619.
(58) Bychkova, V. E.; Dujsekina, A. E.; Klenin, S. I.; Tiktopulo, E. I.; Uversky, V. N.; Ptitsyn, O. B. Molten Globule-Like State of Cytochrome *c* under Conditions Simulating Those Near the Membrane Surface. *Biochemistry* **1996**, *35*, 6058−6063.
(59) Lu, H.; Buck, M.; Radford, S. E.; Dobson, C. M. Acceleration of the Folding of Hen Lysozyme by Trifluoroethanol. *J. Mol. Biol.* **1997**, *265*, 112−117.
(60) Chiti, F.; Taddei, N.; Webster, P.; Hamada, D.; Fiaschi, T.; Ramponi, G.; Dobson, C. M. Acceleration of the Folding of Acylphosphatase by Stabilization of Local Secondary Structure. *Nat. Struct. Biol.* **1999**, *6*, 380−387.
(61) Thomas, P. D.; Dill, K. E. Local and nonlocal interactions in globular proteins and mechanisms of alcohol denaturation. *Protein Sci.* **1993**, *2*, 2050−2065.
(62) Gerlsma, S. Y.; Stuur, E. R. The Effect of Polyhydric and Monohydric Alcohols on the Heat-Induced Reversible Denaturation of Lysozyme and Ribonuclease. *Int. J. Pept. Protein Res.* **1972**, *4*, 377−383.
(63) Tanford, C. Protein Denaturation. *Adv. Protein Chem.* **1968**, *23*, 121−282.
(64) Liu, Y.; Bolen, D. W. The Peptide Backbone Plays a Dominant Role in Protein Stabilization by Naturally Occurring Osmolytes. *Biochemistry* **1995**, *34*, 12884−12891.
(65) Xiong, K.; Asher, S. A. Circular Dichroism and UV Resonance Raman Study of the Impact of Alcohols on the Gibbs Free Energy Landscape of an $\alpha$-Helical Peptide. *Biochemistry* **2010**, *49*, 3336−3342.
(66) Mikhonin, A. V.; Asher, S. A. Direct UV Raman Monitoring of $3_{10}$-Helix and $\pi$-Bulge Premelting during $\alpha$-Helix Unfolding. *J. Am. Chem. Soc.* **2006**, *128*, 13789−13795.
(67) Taboada, P.; Barbosa, S.; Castro, E.; Gutiérrez-Pichel, M.; Mosquera, V. Effect of solvation on the structure conformation of human serum albumin in aqueous−alcohol mixed solvents. *Chem. Phys.* **2007**, *340*, 59−68.